ELSEVIER

Journal of Power Sources 114 (2003) 88–95

JOURNAL OF POWER SOURCES

www.elsevier.com/locate/jpowsour

Characterization of carbon-coated silicon Structural evolution and possible limitations

Nikolay Dimov[a], Kenji Fukuda[b], Tatsuo Umeno[b], Satoshi Kugino[a], Masaki Yoshio[a,*]

[a]*Department of Applied Chemistry, Saga University, 1 Honjo, Saga 840-8502, Japan*
[b]*Mitsui Kozan Co., 1-3 Hibiki, Wakamatsu-ku, Kitakyushu-city, Fukuoka 808-0021, Japan*

Received 14 February 2002; received in revised form 17 September 2002; accepted 25 September 2002

Abstract

Carbon-coated silicon has been synthesized by a thermal vapor deposition method using silicon powder and toluene/benzene vapors carried by a nitrogen carrier gas. It has been investigated under different charging/discharging modes. In all cases, the silicon lattice undergoes gradual destruction during lithium insertion/extraction. Lithium ion extraction from the silicon host matrix did not lead to the formation of an ordered silicon structure. In addition, no new ordered phases were detected. Impedance spectroscopy was applied to monitor the changes during the first lithium insertion/extraction. The results suggest that the material behaves differently than the typical single phase well-defined structures, from which is possible to extract the diffusion coefficient at all lithium insertion levels. Impedance spectra rather detected the phase transition and connected changes in the roughness of the phase boundaries between the Si/C and C/electrolyte. Estimation of the diffusion coefficient was possible only after deeper lithium insertion/extraction when the spectra pattern followed the predictions of the Randless model.

Keywords: Silicon; Lithium battery; Anode material; Impedance spectroscopy

1. Introduction

There are two possible groups of alternatives to graphite anodes for LIB. One extreme group is the recently studied zero-strain anodes as $Li[Li_{1/3}Ti_{5/3}]O_4$ [1]. Because of the perfect match between the binding site in such material and the Li^+ ion, it possesses excellent cycleability over thousands of cycles. However, due to their comparatively high molecular weight, such materials have a capacity of 150 mAh/g a less. On the other extreme, are the elements from the third, fourth, and fifth row of groups III, IV, and V of the periodic table, some of their alloys and oxides. In contrast to the previously mentioned materials, these metals have very high theoretical capacities on the order of 500–4000 mAh/g (for the case of Si) when forming the alloys Li_xM (typically $x = 1-4$). However, due to the volume change and the phase separation of the anodes composed of such materials, they have not been developed into a commercial product. It turns out that during the first Li^+ insertion, the lattice of the corresponding solid material is partly or fully destroyed. Graphite lies between these two extremes and now is the choice for the anode in commercial lithium ion batteries. During the Li^+ insertion, the volume of graphite changes slightly, providing the necessary stability over hundreds of cycles. Thus the difference among these different groups of anodes has become clear. The key factor for the stability of metal/metal alloys based materials, therefore, should be sought in the stability of the phase boundary of the silicon particles and the media where they are dispersed (usually carbon/graphite). To create such a material several methods were proposed. One of them is to use nanosized Si particles (obtained usually by means of Si_xH_y laser ablation) [2,3]. An obvious drawback of this method is that it first gives small amounts of nanosized material, and second, the small particles have a very high surface energy, they stick to each other and it is difficult to disperse them uniformly in the carbon matrix. Recently, a new method has been proposed—the in situ formation of metal nanoclusters [4]. It seems that this technique makes is possible to avoid the drawbacks of the first method. It could be quickly described as heating of an intimate mixture of some metal chlorides (for example $PbCl_2$) with Si or P mixed with the appropriate

* Corresponding author. Fax.: +81-952-28-8591.
E-mail address: yoshio@ccs.ce.saga-u.ac.jp (M. Yoshio).

0378-7753/02/$ – see front matter
PII: S0378-7753(02)00533-5

amount of carbon/graphite. Since the formation of the metal clusters is taking place in the carbon matrix, they are directly embedded in the carbon conducting/supporting media thus avoiding the problem of a high surface energy (sticking) of the separately obtained nanosized particles. This process seems to be promising but its possible drawback might be the poor reproducibility of the samples. That is why we have tested a carbon coating as a method to keep the silicon particles away of each other thus providing reasonable cycling performance. This method was applied to obtain a carbon-coated graphite, having a much better cycling performance than the natural one both in ethylene- and propylene-carbonate based solutions [5]. In addition, it is commercially available and could be applied to a large-scale production.

In this study, we continued our previous work [6]. We have shown that the performance of such a material is strongly dependent on the test conditions. Here the material's properties have been further investigated. The effective diffusion coefficients at certain lithium insertion levels have been estimated and the mechanism of the capacity fading was suggested. The possible limitations in the preparation of this type of anode have also been suggested.

2. Experimental

Carbon-coated silicon was prepared by the Mitsui Kozan Co. (Japan) and used without any further treatment. This material has the following characteristics: mean particle size of 18 μm, tapping density of 0.9 g/cm^3, specific surface area of 2.8 m^2/g, thickness of the carbon layer of 1.25 μm, and the amount of coated carbon 20 wt.%. It was mixed with 10 wt.% PVDF solution in NMP and pasted on a copper foil or stainless mesh welded to a stainless circle. It was then dried at 150 °C for 3 min under a stream of fresh hot air. The resultant weight ratio of the carbon-coated silicon and PVDF was 9:1. From the sheet were punched circle electrodes with an area of 2 cm^2. They were pressed at 500 kg/cm^2 between two stainless steel plates, dried overnight at 140 °C under vacuum and used in the cycling test versus lithium metal. Cell assembling and opening were done in an argon filled glove box. Cycling test was performed using the Nagano test system (Japan) which allows working both in the potentiostatic and galvanostatic modes. Ex situ electrode X-ray diffraction (XRD, Rint 1000, Rigaku) using Cu Kα radiation was employed to identify the silicon crystal phase changes with cycling during a 500 mAh/g capacity cut-off test. Impedance spectra were recorded using three-electrode cells with counter and reference electrodes of lithium metal in a 1 M $LiPF_6$ EC:DMC 1:2 (v/v) solution with a Solartron SI 1287 Electrochemical Interface coupled with an SI 1250 Frequency Response Analyzer.

3. Results and discussion

Figs. 1 and 2 show selected sets of data obtained with the carbon-coated silicon. The cycling performance of the carbon-coated silicon versus Li-metal is compared under

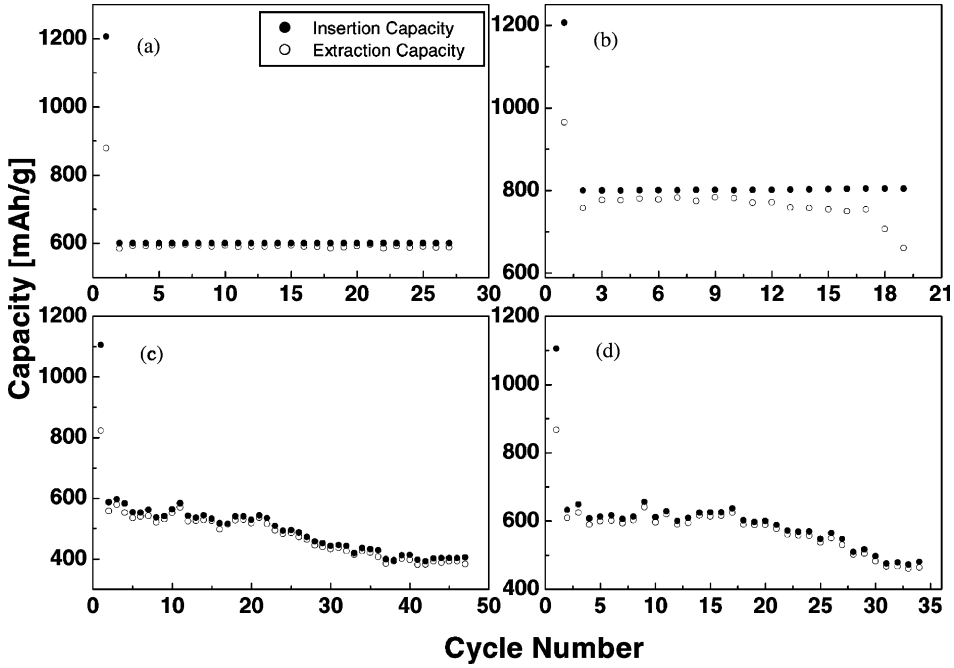

Fig. 1. Capacity/cycle number of carbon-coated silicon cycling test at various conditions: (a) Li^+ insertion: 0.3 mA/mg until 5 mV, then held at 5 mV until 600/1200 (first cycle) mAh/g reached; extraction at 0.3 mA/mg to 1.5 V. (b) Li^+ insertion: 0.3 mA/mg until 5 mV, then held at 5 mV until 800/1200 (first cycle) mAh/g reached; extraction at 0.3 mA/mg to 1.5 V. (c) Li^+ insertion: first cycle 0.3 mA/mg until 5 mV then held at 5 mV until 1100 mAh; next cycles 0.3 mA/mg until 100 mV and held 3 h; extraction at 0.3 mA/mg to 0.8 V. (d) Li^+ insertion: first cycle 0.3 mA/mg until 5 mV then held at 5 mV until 1100 mAh/g; next cycles 0.3 mA/mg until 100 mV and held 3 h; extraction at 0.3 mA/mg to 0.8 V and held at 0.8 V until 0.01 mA/mg.

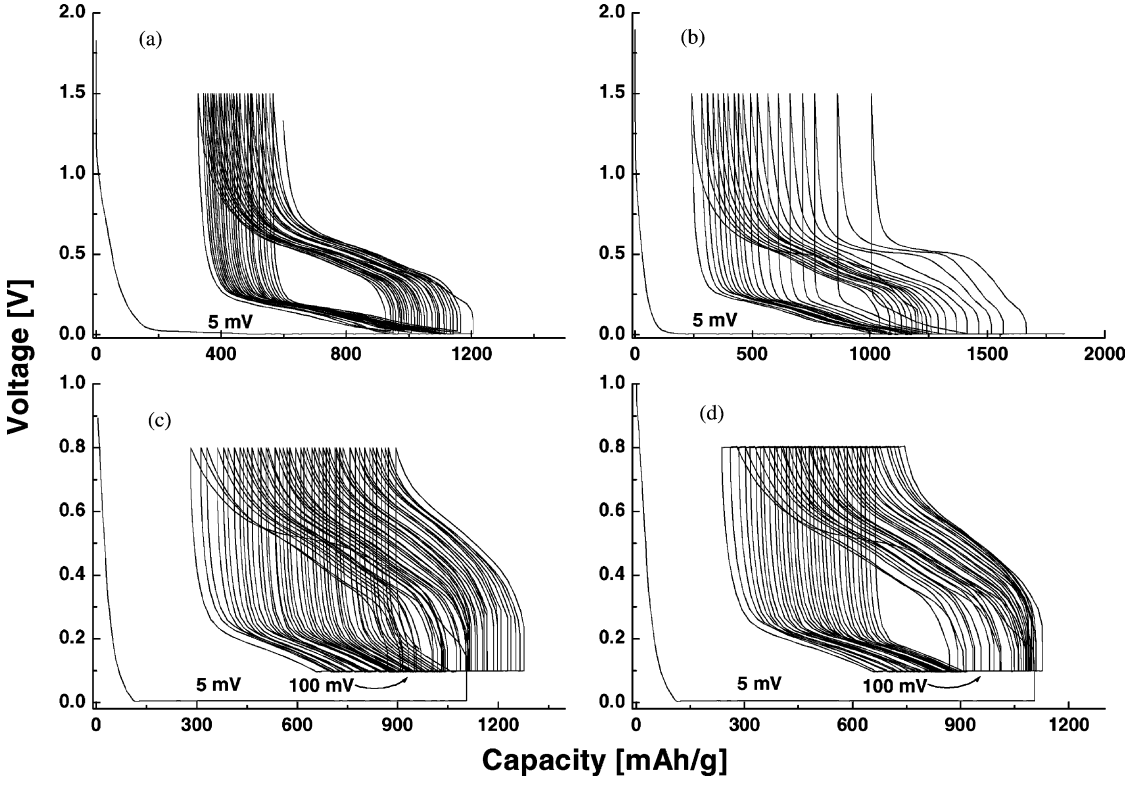

Fig. 2. Voltage/capacity plots of carbon-coated silicon cycling test at various conditions: (a) Li^+ insertion: 0.3 mA/mg until 5 mV, then held at 5 mV until 600/1200 (first cycle) mAh/g reached; extraction at 0.3 mA/mg to 1.5 V. (b) Li^+ insertion: 0.3 mA/mg until 5 mV, then held at 5 mV until 800/1200 (first cycle) mAh/g reached; extraction at 0.3 mA/mg to 1.5 V. (c) Li^+ insertion: first cycle 0.3 mA/mg until 5 mV then held at 5 mV until 1100 mAh; next cycles 0.3 mA/mg until 100 mV and held 3 h; extraction at 0.3 mA/mg to 0.8 V. (d) Li^+ insertion: first cycle 0.3 mA/mg until 5 mV then held at 5 mV until 1100 mAh/g; next cycles 0.3 mA/mg until 100 mV and held 3 h; extraction at 0.3 mA/mg to 0.8 V and held at 0.8 V until 0.01 mA/mg.

different conditions. In all cases, the first charge (corresponding in this case to Li^+ insertion) was 1100/1200 mAh/g with respect to the overall active material mass. It was performed in such a way because of the importance of the first Li^+ insertion step. Otherwise, the capacity/cycle number plots show a distinctive maximum and it is difficult to compare the material's cycling performance at different conditions. Charging was performed as follows. Initially, the current was held at ~0.3 mA/mg until the voltage dropped to 5 mV. Then the voltage was held at 5 mV and the current was decreased accordingly to keep the 5 mV until the predefined capacity was reached (1100 or 1200 mAh/g). From the second cycle, charging was conducted as indicated on the graphs. Li^+ extraction was performed at constant current density (~0.3 mA/mg) until 1.5/0.8 V. Only in (d) case after reaching 0.8 V, the extraction was continued until the current dropped to ~0.01 mA/mg. As mentioned in Section 1, during this step, the main phase transformation of the host matrix into an amorphous phase is taking place. This process needs more energy for the crystal lattice destruction during which the voltage is kept 5 mV. From the second cycle, the final charging/discharging voltage was kept as indicated in Fig. 2. To check whether the extraction process is reversible, different modes have been tested. Dahn and co-worker [9] suggested that decreasing the extraction potential down to 0.8 V leads to enhancement of the cycling performance. However, from the "necked" charging/discharging curves, it is clear that the lower extraction potential does not improve the extraction efficiency. Right side shifting with cycles of the charging peaks is of the same order as for the other cases. From the graphs, we can see that approximately at 1000 mAh/g, the accumulated irreversible capacity fade stops the process. This effect is more pronounced at constant capacity cut-off tests (Figs. 1a, b and 2a, b).

Prior to our studies, there are at least three known reasons causing this inevitable effect: (i) growth of SEI layer; (ii) detachment of the active material from the current collector and (iii) possible irreversible accumulation of Li^+ in the silicon matrix. In all cases, reasonable cycling performance (of the order of tents of cycles) was achieved when the charging during cycling was less than 800 mAh/g. Hence, we can estimate the limiting mole fraction of Li^+ inserted into the Si matrix which still allow reasonable cycling performance. Chemically, the carbon-coated silicon consists of carbon and Si. For the reaction:

$$x\,Li^+Si + x\,e^- \leftrightarrow Li_xSi,$$

we can easily find the relation between the measured capacity, Cap (mAh/g), of the material and the mole fraction of Li^+ [x] inserted in the silicon host matrix. If the amount of

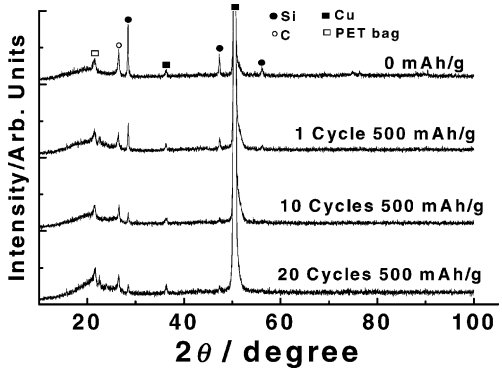

Fig. 3. XRD-data: constant capacity cycling test (500 mAh/g) after different number of cycles.

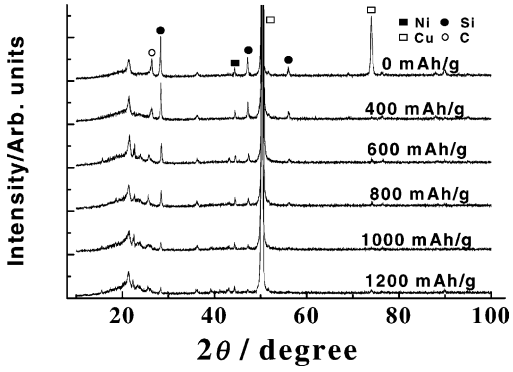

Fig. 4. XRD-data: first Li^+ insertion at various levels (mAh/g).

Si in the material is p [wt.%], the relation could be represented by the equation:

$$\text{Cap} = \frac{26800px}{28.09}, \quad (1)$$

where 28.09 (g/mol) is the atomic mass of silicon.

The latter equation is valid only if there is no parallel insertion of Li^+ into the carbon-phase of the material. However, our previous XRD data [6] suggest that there is some changing of the carbon peak positions, caused by the changes in the carbon-phase. Therefore, we should estimate the contribution of the possible parallel reaction $Li^+ + C_6 + e^- \leftrightarrow LiC_6$. If one considers the maximum capacity of the carbon as equal to 370 mAh/g, the estimate of x in Li_xSi will be:

$$\text{Cap} - (1-p)370 = \frac{26800px_1}{28.09}. \quad (2)$$

Solving the previous equations with respect to x and x_1, we can find the corresponding mole fractions of Li^+ in the silicon host matrix at a given capacity. The previous considerations show that the true value of x should lie in the range $x_1 < x_{\text{real}} < x$. For the material tested here $p = 45\%$, and the limiting capacity is about 800 mAh/g. Substituting the numbers into Eqs. (1) and (2), we find $x = 1.86$, $x_1 = 1.38$. The same estimation for the case of the first Li^+ insertion (1200 mAh/g) gives $x = 2.8$ and $x_1 = 2.3$. From the Li–Si-phase diagram one can see that there are some possible alloy compositions existing at elevated temperatures: $Li_{1.71}Si$, $Li_{2.33}Si$, $Li_{3.25}Si$ and $Li_{4.4}Si$. Therefore, in this case, reasonable cycling performance was achieved working with the lowest and medium lithium content alloy (i.e. $Li_{1.71}Si$ or $Li_{2.33}Si$). The estimations performed so far suggest that Li^+ uniformly reacts with the bulk of the silicon particles. However, it is likely that during the Li^+ insertion (specially at the high current density, we normally apply ≈0.3 mA/mg) the surface layer is supersaturated with Li^+, while in the center of the particle remains partly or fully unchanged region of fresh silicon. During cycling, this silicon core undergoes gradual amorphization and the distribution of the amorphous area is becoming uniform. Evidence for this hypothesis is the XRD pattern of the material cycled during the 500 mAh/g capacity cut-off test presented in Fig. 3. Material was cycled as follows: Charging (Li^+ insertion) was performed until 500 mAh/g, and discharging (Li^+ extraction) at 0.3 mA/mg until 1.5 V were reached. Prolonged cycling at 500 mAh/g lead to a gradual decrease in the intensity of the Si-related peaks. The same changes are observed during the first cycle at heavier insertion levels. The XRD-data for the latter case are given in Fig. 4 for comparison. It is also noticed that in both cases there are no newly formed peaks. Forming of an "XRD-transparent" material means that the mechanism of the chemical high temperature reaction and low temperature electrochemical reaction is different. In the first case, we can obtain a well-defined structure, in the latter one, only a highly amorphous phase with near ordering. The same conclusion was drawn in [7], where Li^+ insertion in the silicon host matrix was studied in detail using various techniques (HRETM, Raman spectroscopy, SEM) and it was shown that the lithium ions inserted in the silicon matrix lead to destruction of the silicon lattice. In addition, the silicon nanoparticles dispersed within carbon black media have agglomerated into dense blocks. The process known as electrochemical sintering [8] was supposed to be responsible for the fast capacity fade. On the other hand, the presence of intrinsic (in the case of nanoparticles, studied in [7]) and insertion-generated defaults within the silicon matrix can produce some amount of dangling bonds. Thus the structural stability of the silicon anodes should be separated into two distinct problems: (i) morphological stability of the particles, and (ii) reversibility of the lithium insertion/extraction reaction.

To explore in more detail the material behavior, impedance spectroscopy has been applied. The standard equivalent circuit used to represent a diffusion controlled electrochemical process is the Randless equivalent circuit. Originally, this method was developed to find the chemical diffusion coefficients of electrochemical species in solid state thin films [10]. In our case, however, the situation is much more complicated. We have an Si particle covered by a carbon layer. Therefore, one may expect peculiarities because of the presence of phase

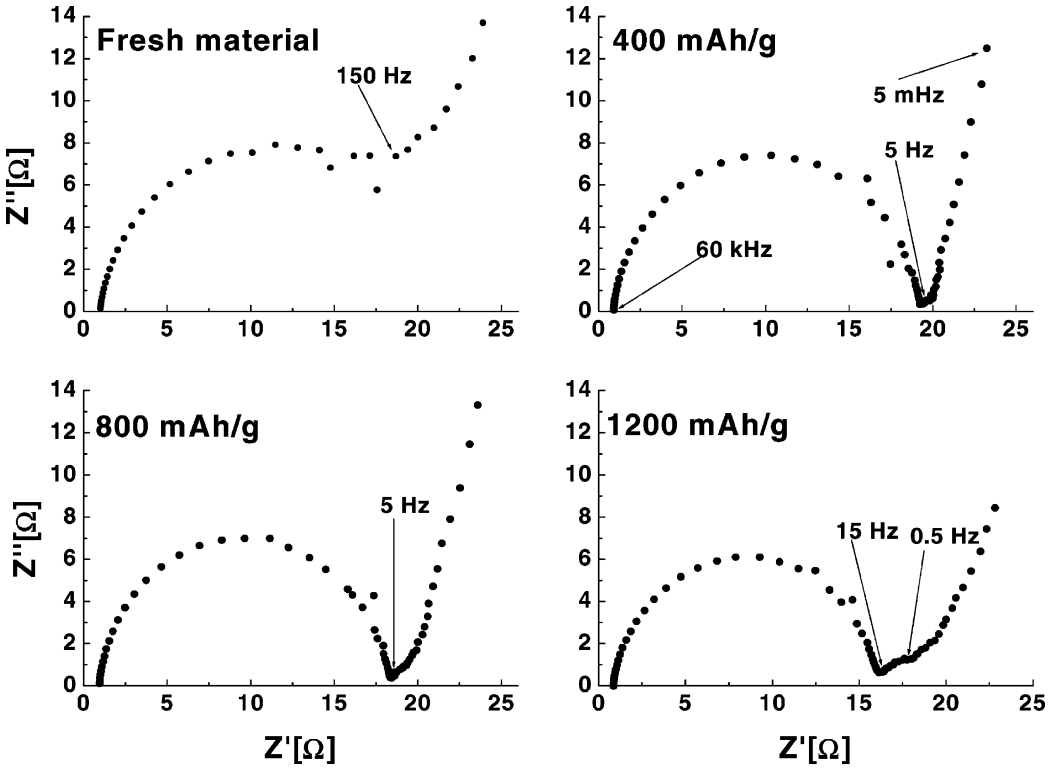

Fig. 5. Impedance spectra of carbon-coated silicon after the first Li^+ insertion at different insertion levels indicated on the graphs.

boundaries i.e. C/electrolyte, Si/C and eventually Si/electrolyte. In addition, because of the spatial distribution of the solid phases (central Si core covered by carbon layer), one may expect preferred insertion of Li^+ in the carbon-phase at the beginning of the process.

Fig. 5 represents the impedance spectra of the carbon-coated silicon. Charging was conducted at a low current density (50 μA/cm^2 or 10 μA/mg) to ensure near equilibrium conditions. After charging to some capacity (marked on the graphs), the cells were rested for 5 h. Impedance spectroscopy measurements were performed over a frequency range from 5 mHz to 60 kHz. The ac amplitude used during the measurements was 10 mV. Fig. 6 shows the same material after the first Li^+ extraction. It was performed until the cell voltage reached 1.5 V. A fresh sample spectrum is given in both figures at different magnifications since its values are much higher compared to the other samples at the lower frequencies.

As noted in [10], the diffusion coefficient can be determined from the low frequency region, where the diffusion impedance dominates. In this region and when the condition $\kappa l \gg 1$ (where $\kappa = (\omega/2\mathrm{D})^{1/2}$), l: thickness of the film) also applies, a plot of Im(Z) versus Re(Z) gives a straight line with a slope of 45°. Under such conditions, the expression for the Warburg impedance simplifies to $\mathrm{Re}(Z) = \mathrm{Im}(Z) = \text{slope} * \omega^{-1/2}$, where the slope is expressed as $V_\mathrm{m}(\mathrm{d}E/\mathrm{d}x)/nFS(2D)^{1/2}$. Hence the diffusion coefficient under such conditions can be extracted from a plot of Re(Z) vs. $\omega^{-1/2}$ or Im(Z) vs. $\omega^{-1/2}$. The frequency range used depends on the structure of the material, as the condition $\kappa l \gg 1$ must be satisfied. This is experimentally found by examination of the data. The intercept for Re(Z) corresponds to the sum of the charge transfer resistance and electrolyte resistance. The intercept for Im(Z) (corresponding to $\omega \rightarrow \infty$) is expected to be zero. Only when there is an agreement between the slopes of both lines (Re(Z)/$\omega^{-1/2}$, Im(Z)/$\omega^{-1/2}$) and the slope of the Cole–Cole plot is reasonably close to 1 (45°), we can estimate the diffusion coefficient.

However, for a finite film thickness, a straight behavior is not always observed, and a second semicircle can be seen in the Im(Z)–Re(Z) plot. This corresponds to a second process taking place at the film substrate interface. The condition for the observation of this process is $l^2 < D/\omega$.

Looking at the actual data, we can see that increasing the charging level is accompanied by changes in the spectral pattern. In the three charged states, the spectra is represented by depressed semicircles and a linear portion. However, the slope with the real axis is substantially bigger than 45°. Interestingly, after charging these three samples show different behavior. The sample charged to 400 mAh/g shows two depressed semicircles followed by a linear portion. It slope with the real axis is still much higher than 45°. On the other hand, the samples operated at 800 and 1200 mAh/g show linear portions with a slope near 45° which reasonably matches the Randless model. The sample at 800 mAh/g has a small second semicircle, but this effect is not well pronounced. In summary, the second semicircle gradually disappears as the lithium insertion level increases. We

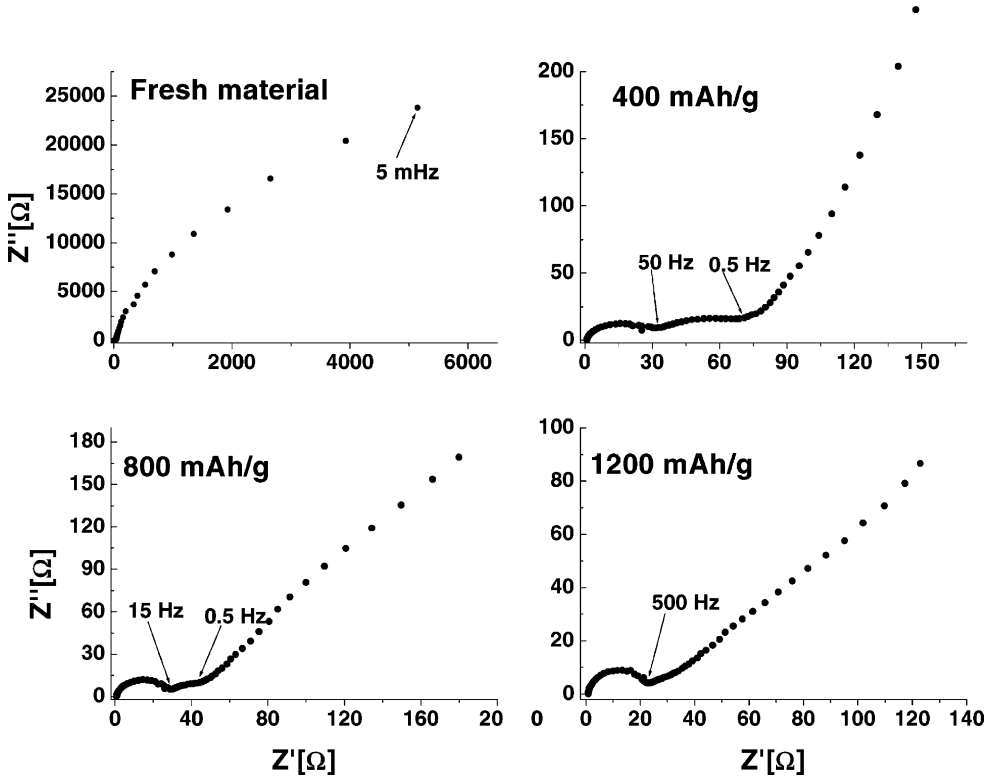

Fig. 6. Samples shown on Fig. 5 after Li^+ extraction at 0.3 mA/mg until 1.5 V was reached.

explain these data in the following way. The fresh sample has much higher impedance at the low frequencies, which is most probably a consequence of its fractional dimension characteristic. When lithium ion insertion starts there is a compression of the carbon layer caused by the silicon matrix expansion. Since this is not a single-phase material, it deviates from the classic prediction. When extraction starts, the difference between the samples becomes even more pronounced. The difference between the 400 mAh/g sample and the other two samples is probably caused by the preferred lithium insertion in the carbon-phase at the beginning of the process. At a low initial charging level, the contact between the silicon and carbon-phase is not good. The second semicircle is related to the fractional characteristic of the rough phase silicon/C boundary. At higher charging levels, however, the contact between these both phases becomes better and the material as a whole behaves as single-phase material. We can estimate the diffusion coefficient in these particular cases. The molar volume of silicon is 12 cm^3/mol and that of graphite 5.5 cm^3/mol. Since lithium insertion simultaneously takes place in both phases, the effective molar volume of the material should lie between these two values. If we take the amount for silicon, the respective diffusion coefficient for levels of 800 and 1200 mAh/g are 1.7×10^{-11} and 6.0×10^{-11} cm^2/s. Keeping in mind the obstacles mentioned above, we do not expect to get the exact values of the diffusion coefficient. For us is more important to see the trend and the general behavior as the lithium insertion level increases. The only cases when we can apply with some degree of certainty the calculation of the diffusion coefficient value are the samples charged to 800 and 1200 mAh/g and then discharged to 1.5 V. Their close values confirm our hypothesis for the importance of the silicon lattice destruction during the first lithium insertion. At the beginning of the process, the material strongly deviates from the usual predictions. The difference in the slopes of Re(Z) and Im(Z) for the light Li^+ insertion level is clear evidence for this hypothesis. On the other hand, the heavier insertion levels show reasonably close values. Another interesting point to notice is the value of the intercept $Z_{Re}/\omega^{-1/2}$. During the insertion, it does not change signifficantly, which indicates there is no considerable SEI-layer formation. After the extraction, the Z_{Re} intercepts are scattered. The sample at the light insertion level deviates most strongly from its previous value. Although the reason is not clear yet, it is likely that this is due to the roughness of the Si/C-phase boundary. At 400 mAh/g, the estimated value of x is 0.2. At such a low content the carbon layer is not pressed yet, but at the same time, it is likely that the Si surface roughness is higher than in the initial state. As a result, the condition $l^2 < D/\omega$ is probably satisfied and, the impedance spectra show the typical second semicircle. The physical meaning of l in this case is the typical dimension of the roughness on the silicon surface. The data are summarized in Table 1. The respective slopes and intercepts are given with the accuracy determined by the linear fitting procedure. R is the correlation coefficient, and n is the number of points involved in the fitting procedure (i.e.

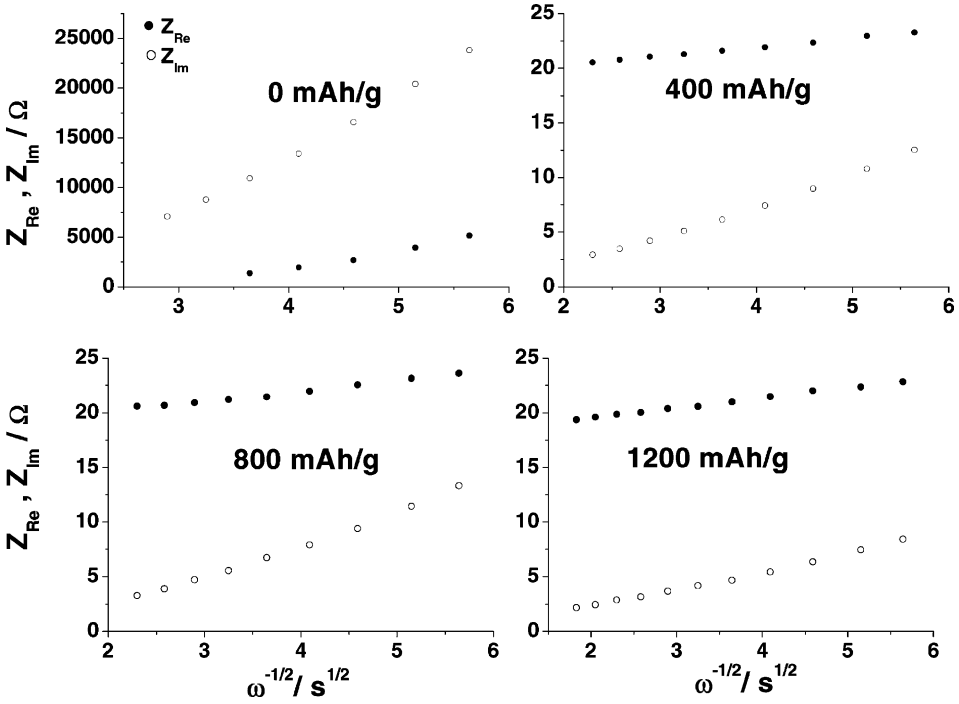

Fig. 7. Z_{Re}/Z_{Im} vs. $\omega^{-1/2}$ plots of the data presented on Fig. 5.

the points lying on a straight line at the lowest frequency range). Estimation of the diffusion coefficient value was performed only when the main assumptions of the theory were met (Cole–Cole linear portion angle close to 1 (45°), close to the values of the slopes $Z_{Re}/\omega^{-1/2}$; $Z_{Im}/\omega^{-1/2}$). The impedance spectra of the carbon-coated silicon and the results extracted from them are given on Figs. 5–8. The estimation of the amount of Li^+ inserted in the Si matrix was based on the assumption, that Li^+ first saturates the carbon layer and then is getting into the silicon. A possible reason for the better matching of the data with the Randless model at higher Li^+ insertion levels is the uniform nature of the

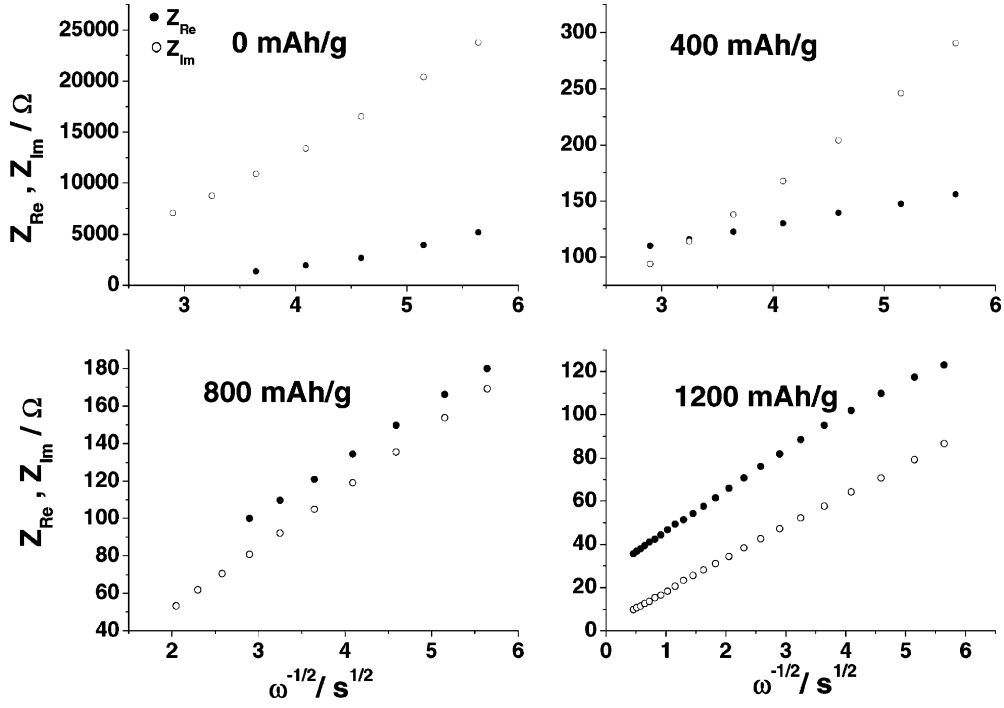

Fig. 8. Z_{Re}/Z_{Im} vs. $\omega^{-1/2}$ plots of the data presented on Fig. 6.

Table 1
Summary of the impedance spectra data

Insertion (mAh/g)	Slope			Intercept		R	n	$D_{eff} \times 10^{-11}$ (cm^2/s)
	Cole–Cole	$Z_{Re}/\omega^{-1/2}$ ($\Omega\ s^{-1/2}$)	$Z_{Im}/\omega^{-1/2}$ ($\Omega\ s^{-1/2}$)	$Z_{Re}/\omega^{-1/2}$ (Ω)	$Z_{Im}/\omega^{-1/2}$ (Ω)			
0	–	–	–	–	–	–	–	–
400 ($\cong Li_{0.2}Si$)	3.49 ± 0.09/74.0 ± 0.4°	0.82 ± 0.02	2.87 ± 0.08	18.61 ± 0.07	−4.06 ± 0.31	0.998	9	–
800 ($\cong Li_{1.5}Si$)	3.17 ± 0.09/72.5 ± 0.5°	0.93 ± 0.04	2.97 ± 0.09	18.25 ± 0.15	−3.19 ± 0.37	0.996	9	–
1200 ($\cong Li_{2.5}Si$)	1.78 ± 0.05/60.7 ± 0.6°	0.91 ± 0.01	1.62 ± 0.04	17.7 ± 0.05	−0.98 ± 0.16	0.998	11	–
After Li^+ extraction								
Sample 400	4.24 ± 0.16/76.7 ± 0.5°	16.76 ± 0.21	71.23 ± 2.33	61.51 ± 0.91	−118.67 ± 9.63	0.998	7	–
Sample 800	1.14 ± 0.02/48.7 ± 0.5°	29.42 ± 0.22	32.31 ± 0.05	14.12 ± 0.88	−12.92 ± 0.18	0.999	10	1.7
Sample 1200	0.85 ± 0.01/40.4 ± 0.3°	17.49 ± 0.21	14.85 ± 0.08	28.84 ± 0.60	3.34 ± 0.21	0.999	23	6.4

material after the first insertion/extraction. During the first insertion, it is likely that there is a big concentration gradient of Li^+ in the bulk of the silicon core. After the extraction, the residual Li^+ ions are uniformly distributed within the newly formed amorphous phase. In addition because of the volume expansion, the carbon layer is pressed and the material effectively shows a single-phase solid state behavior.

4. Conclusions

By covering the silicon particles with carbon, the cycling performance of anodes was substantially improved. The obtained results are comparable with the ones obtained using more difficult methods. The material shows a high reversible capacity over 600 mAh/g for the first 25 cycles. To determine whether this class of materials will be able to replace carbon, the mechanism of the capacity fading (of the order of 5–10 mAh/g per cycle) should be studied in more detail, which is currently in progress. Our previous data [6] suggest that the carbon coating is an effective method to preserve the integrity of the particles. However, this might be not enough to have long term cycling performance. After densification of the carbon layer, the silicon core (in this case with diameter of the order of 10 μm) does not merge with the other particles, but it probably accumulates some amount of Li^+. In view of these findings, further improvement of the material probably should be done in two ways:

(i) finding the limitations imposed by the nature in terms of particle size (if any), under which one may have satisfactory cycling performance; and
(ii) finding some alloys (probably highly amorphous in their initial state) which might be able to alloy reversibly with lithium ions.

References

[1] T. Ohzuku, T. Wada, S. Yamamoto, K. Ariyoshi, in: Proceedings of The 42nd Battery Symposium in Japan, Yokohama, 21–23 November, Session 3A19.
[2] H. Li, X. Huang, L. Chen, Z. Wu, Y. Liang, Electrochem. Solid State Lett. 2 (11) (1999) 547–549.
[3] I. Kim, P. Kumta, G.E. Blomgren, Electrochem. Solid State Lett. 3 (11) (2000) 493–496.
[4] G.A. Nazri, in: Proceedings of the Abstract 249 of Joint International Meeting, San Francisco, CA, 2–7 September 2001.
[5] M. Yoshio, H. Wang, K. Fukuda, Y. Hara, Y. Adachi, J. Electrochem Soc. 147 (4) (2000) 1245–1250.
[6] T. Umeno, K. Fukuda, H. Wang, N. Dimov, T. Iwao, M. Yoshio, Chem Lett. (2001) CL-010828.
[7] H. Li, X. Huang, L. Chen, G. Zhou, Z. Zhang, D. Yu, Y.J. Mo, N. Pei, Solid State Ionics 135 (2000) 181–191.
[8] J.T. Vaughey, K.D. Keplar, D.R. Vissers, M.M. Thackeray, in: Proceedings of the Abstracts of the Ninth International Meeting on Lithium Batteries, Poster 1, Tues 82, Edinburgh, Scotland, July 1998.
[9] I.A. Courtney, J.R. Dahn, J. Electrochem. Soc. 144 (1997) 2943.
[10] C. Ho, I.D. Raistric, R.A. Huggins, J. Electrochem. Soc. 127 (1980) 343–350.